

The effect of a dipping layer on the first-arrival traveltime from zero-offset and fixed-offset borehole radar

Dale Rucker¹ and Ty P.A. Ferré²

¹ hydroGEOPHYSICS, Inc., 2302 N Forbes Blvd, Tucson, AZ 85745, USA

² Department of Hydrology and Water Resources, University of Arizona, Harshbarger Building 11, PO Box 210011, Tucson, AZ 85721, USA

Received September 2004, revision accepted September 2006

ABSTRACT

The effect of a dipping layer on the first-arrival traveltime from single-offset profiling with borehole radar is investigated, including both zero-offset and fixed-offset profiling. In our study, offset refers to the vertical distance between bistatic radar antennae. Using forward modelling of electromagnetic wave travel, the traveltime of zero-offset and fixed-offset profiles through a dipping layer is compared to those of flat-lying layers. The model considers three distinct raypaths: direct, critically refracted and cross-dip refracted. Whereas critical refraction only occurs in a layer of low propagation velocity relative to an adjacent high-velocity layer, cross-dip refraction can occur in any velocity structure. The forward model demonstrated that the slope of the traveltime through the cross-dip portion of the profile is approximately half of that in the critically refracted portion. To obtain the electromagnetic wave propagation velocities above and below the dip, only one profile is necessary. However, to invert for the dip angle and position, two profiles with different offsets must be considered together.

INTRODUCTION

Profiling with borehole ground-penetrating radar (BGPR) is a method by which the vertical distribution of the electromagnetic wave propagation velocity of soil can be obtained from multiple measurements of first-arrival traveltime between a transmitting and a receiving antenna. The relative apparent dielectric permittivity of the medium, which is relevant to several properties of hydrological significance (Day-Lewis, Harris and Gorelick 2002), is then related to the propagation velocity (Davis and Annan 1989; Cai and McMechan 1995). Data acquisition for BGPR can be obtained in one of several modes, including a multi-offset or single-offset gather, where offset refers to the vertical separation between the bistatic radar antennae (Redman, Parkin and Annan 2000). A multi-offset gather offers multidimensional imaging of the dielectric permittivity through high-resolution tomography (Lager and Lytle 1977) by making measurements at many vertical offsets of the antennae (see e.g. Jackson and Tweeton 1994; Nekut 1994; Vasco, Peterson and Lee 1997; Holliger, Musil and Maurer 2001). The collection time, however, is long for a multi-offset gather. For example, Alumbaugh *et al.* (2002) reported a six-hour acquisition time for four profiles to 7 m depth with a 0.25 m vertical sampling interval. In a single-offset gather, where one shot is made per depth location, the result is a rapid one-dimensional profile of the subsurface (e.g. Davis and Annan 2002).

Rapid data acquisition may be important in highly transient subsurface processes, such as infiltration of water during ephemeral stream flow. During the single-offset gather, lateral discontinuities of velocity are averaged arithmetically to obtain an average traveltime along the path (Chan and Knight 1999). Single-offset gathers may be collected in either zero-offset or fixed-offset profiling modes. In zero-offset profiling, the transmitting and receiving antennae are located at the same depth below ground. In fixed-offset profiling, the transmitting and receiving antennae are located at different depths.

In situations of simple flat-lying layered media, a multi-offset gather is unnecessary. The one-dimensionality of the earth can be captured adequately with a zero-offset profile, provided the correct travelpath is recognized. Rucker and Ferré (2003) identified situations where electromagnetic waves will not travel directly between the antennae, for example near the ground surface. The contrast in propagation velocity will cause the electromagnetic waves to be refracted critically at the boundary between air and soil. Correcting for critical refraction is necessary to characterize the subsurface properly. In a two-dimensional earth, where a dipping layer may exist, a zero-offset profile may obscure the details of the subsurface, making interpretation difficult. The dipping layer will cause the electromagnetic wave to be refracted at various angles when shooting across the dip. The stratigraphy, however, is still comprised of layered sediments. A complete multi-offset gather, where traveltimes from all offsets are

* dale@hydrogeophysics.com

measured, remains unnecessary. In this case, a fixed-offset profile with an offset that allows profiling with or against the dip angle can be used. However, to discern both location and angle of dip, two profiles with different offsets are needed.

Rucker and Ferré (2003, 2004) presented solutions for travel-time inversion to obtain the propagation velocity for flat-lying layers using zero-offset profiling. The inversion was straightforward because only two modes of electromagnetic wave travel are possible: direct and critically refracted. The correction for critical refraction uses the slope of the traveltime curve with depth in regions where the traveltime exhibits a linear change with depth. The slope is related to the velocity where critical refraction occurs. Their analysis did not include the effects of a dip on the traveltime measured by zero-offset profiling. Subsurface layers are seldom flat. Therefore, we present the solution of a forward model for traveltime through a single dipping layer using ray-tracing analysis. Additionally, we demonstrate a method by which the traveltime can be inverted to obtain the velocity above and below the dip, the dip location and the dip angle. The method is applied to both synthetic and field-collected data. The results of the field data are compared with the interpretation of soil cores and borehole logs of neutron counts and electrical conductivity.

THEORY

Forward traveltime calculations

Consider single-offset profiling across a low-velocity dipping layer. The layer geometry is defined by its depth midway between the antennae (z_{dip}) and the angle of inclination from the horizontal (α). The layer is located sufficiently far below ground so that first-arriving critical refraction does not occur along the ground surface. Figure 1 shows the travelpaths of electromagnetic waves when $v_1 > v_2$, where v_1 is the velocity above the dip and v_2 is the velocity below the dip. When both the transmitter (Tx) and the receiver (Rx) are above the dip, the travelpath is direct (position 1 in Fig. 1).

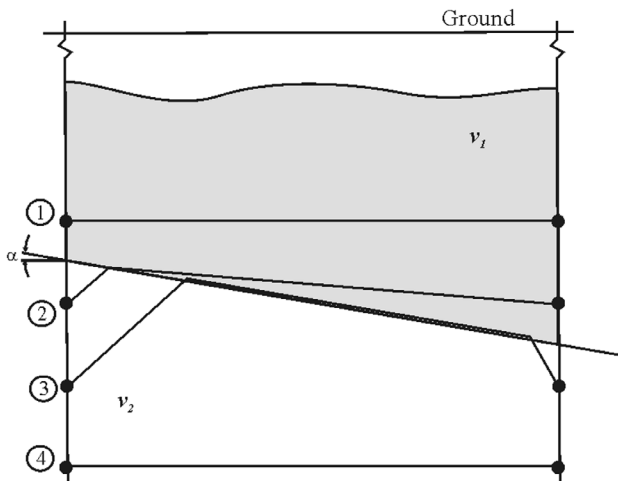


FIGURE 1 Four positions of the borehole antennae during profiling of dipping layer with zero-offset and fixed-offset profiling BGPR.

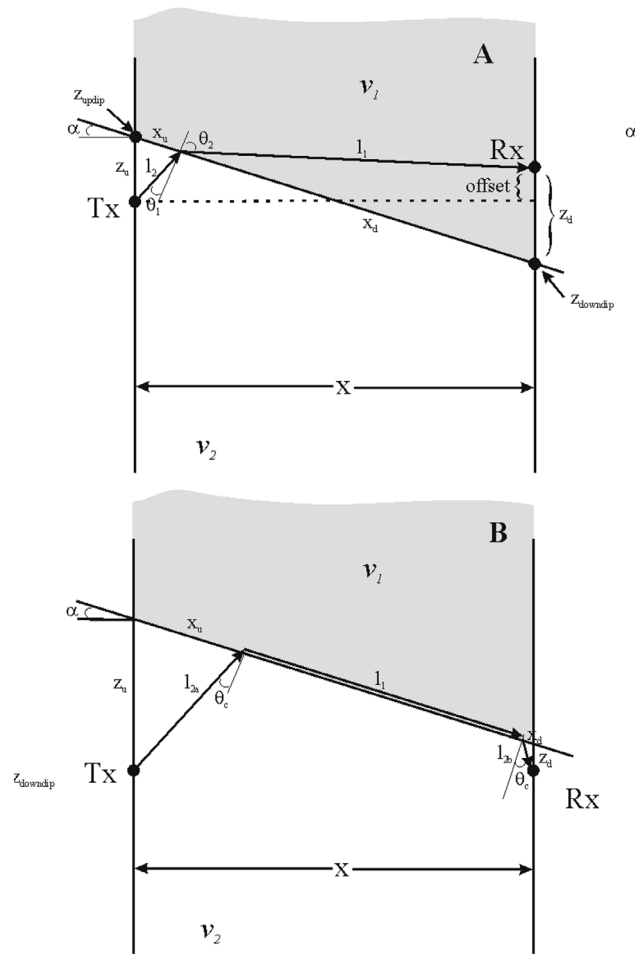


FIGURE 2 (a) Geometric considerations of profiling across a dipping layer. (b) Geometric consideration of critical refracted traveltime with a dipping layer present.

As the antennae straddle the dip, the cross-dip travelpath is refracted at the interface between the two layers (position 2). As the antennae move below the dip, the travelpath is critically refracted along the interface, and a portion of the wave travels in both layers (position 3). Finally, when the antennae are well below the dip, the travelpath returns to being direct (position 4).

To calculate the traveltime for each position of the antennae, the pathlengths travelled through each layer are needed. For position 1, the traveltime (τ_1) is given by

$$\tau_1 = \frac{\sqrt{x^2 + offset^2}}{v_1}, \tag{1}$$

where x is the antennae separation distance and $offset$ is the vertical offset of the antennae centres (positive downwards). Using Fig. 2(a) as a guide, the traveltime through the cross-dip (position 2) is given by

$$\tau_2 = \frac{l_2}{v_2} + \frac{l_1}{v_1}, \tag{2}$$

where l_2 is the pathlength travelled in the layer described by v_2 , and l_1 is the pathlength travelled in layer v_1 . The values of l_1 and l_2 can be computed considering the law of sines:

$$l_u = z_u \frac{\cos(\alpha)}{\cos(\theta_1)} \quad (3)$$

and

$$l_d = z_d \frac{\cos(\alpha)}{\cos(\theta_2)}. \quad (4)$$

The variable z_u is defined as the vertical distance between the centre of the transmitting antenna (z_{Tx}) and the intersection of the dip interface with the transmitter access tube (z_{updip}); z_d is the vertical distance between the receiving antennae (z_{Rx}) and the intersection of the dip interface with the receiver access tube (z_{downdip}). The unknowns in equations (3) and (4) are the angles of incidence (θ_1) and refraction (θ_2) at which the electromagnetic waves arrive and leave the interface. These angles will depend on the velocity ratio of the two layers and the location along the interface where the ray enters layer 1 from layer 2:

$$\theta_1 \cong \cos^{-1} \left[\left(1 - \frac{v_2^2}{v_1^2} + \frac{v_2^2}{v_1^2} \left(\frac{\cos(\alpha) z_d}{x - z_u \cos(\alpha)} \right)^2 \right)^{1/2} \right], \quad (5)$$

$$\theta_2 = \sin^{-1} \left(\frac{v_1}{v_2} \sin(\theta_1) \right). \quad (6)$$

The complete derivation of θ_1 is given in Appendix A.

For position 3, the total traveltime is defined by the travel along three pathlengths, l_u , l_d and l_m :

$$\tau_3 = \frac{l_{2a} + l_{2b} + l_1}{v_2}, \quad (7)$$

where l_1 (Fig. 2b) is the pathlength travelled along the boundary through the high-velocity layer due to critical refraction. The three travelpath lengths in equation (7) are

$$l_{2a} = z_u \frac{\cos(\alpha)}{\cos(\theta_c)}, \quad (8)$$

$$l_{2b} = z_d \frac{\cos\left(\frac{\pi}{2} + \alpha\right)}{\cos(\theta_c)} \quad (9)$$

and

$$l_1 = \frac{x}{\cos(\alpha)} - z_u \frac{\sin(\theta_c + \alpha)}{\cos(\theta_c)} - z_d \frac{\sin(\theta_c - \alpha)}{\cos(\theta_c)}. \quad (10)$$

The critical angle (θ_c) according to Snell's law is given by

$$\theta_c = \sin^{-1} \left(\frac{v_2}{v_1} \right). \quad (11)$$

Lastly, as the antennae pass into position 4, the direct traveltime is

$$\tau_4 = \frac{\sqrt{x^2 + \text{offset}^2}}{v_2}. \quad (12)$$

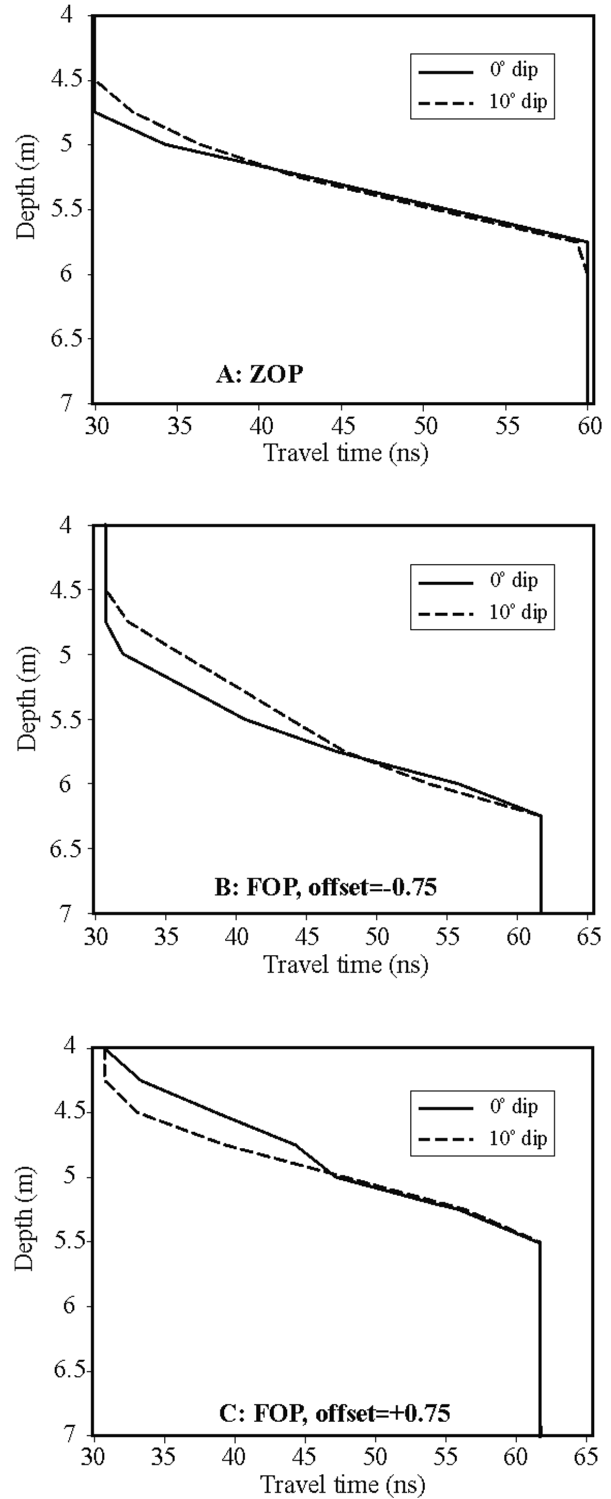


FIGURE 3 Forward modelling of traveltimes across a dipping interface. (a) Zero-offset profiling (ZOP) across interfaces with dip angles of 0° and 10° . (b) Fixed-offset profiling (FOP) with an offset of -0.75 m across interfaces with dip angles of 0° and 10° . (c) Fixed-offset profiling with an offset of $+0.75$ m across interfaces with dip angles of 0° and 10° .

The depth at which the critically refracted traveltime is equal to the direct traveltime for a zero-offset profiling measurement is referred to as the refraction termination depth, z_{rd} . For depths greater than z_{rd} , the direct arrival (τ_4) is the first-arrival (Rucker and Ferré 2003). For a dipping layer, the value of z_{rd} will depend on the velocities above and below the dip, the dip angle and the offset. For zero-offset, z_{rd} is given by

$$z_{\text{rd}} = \frac{x \frac{v_1}{\cos(\alpha)} - v_2}{2 \sqrt{v_1^2 - v_2^2}}. \quad (13)$$

To demonstrate the solution for a first-arrival traveltime profile through a dipping layer, the traveltime with zero-offset profiling BGPR from two geometries of differing dip angles ($\alpha=0^\circ$ and 10°) are shown (Fig. 3). The dip is located at $z_{\text{dip}}=4.875$ m and the antennae separation is 3 m. For reference, a 10° dip creates a difference in the location of the interface of 0.53 m over a 3 m separation. The zero-offset profiling BGPR measurements are made with a sampling interval of 0.25 m and span depths from 4 m to 7 m. The velocity above the dip is 0.1 m/ns and the velocity below the dip is 0.05 m/ns. Figure 3(a) shows that the traveltime profiles are almost identical everywhere except in the depth range from 4.5 m to 5 m. This difference is caused by the cross-dip traveltimes in a layer with dip.

Figure 3(b, c) shows the traveltimes from fixed-offset profiling with offsets of -0.75 m and $+0.75$ m, respectively. In Fig. 3(b), with the receiving antenna above the transmitting antenna, the antennae straddle the dip for a much longer period than in Fig. 3(c). The effect is a traveltime profile that exhibits fewer direct traveltime measurements (positions 1 and 4 in Fig. 1) than in Fig. 3(a). In Fig. 3(c), with the receiving antenna lower than the transmitting antenna, cross-dip traveltimes only occur for the flat-lying layer. For the 10° dip case, the antennae are coincident with the dip angle, and no cross-dip traveltimes occur.

TABLE 1
Traveltime slope calculations

v_1 (m/ns)	v_2 (m/ns)	Dip ($^\circ$)	Offset (m)	Cross-dip slope (ns/m)	Critical refraction slope (ns/m)
0.1	0.05	0	0	--	34.64
0.1	0.05	10	0	16.24	34.11
0.1	0.05	0	-0.75	17.32	34.64
0.1	0.05	10	-0.75	15.34	34.11
0.07	0.05	0	0	--	27.99
0.07	0.05	10	0	12.57	27.65
0.07	0.05	0	-0.75	14.02	27.99
0.07	0.05	10	-0.75	11.36	27.56

Inversion of traveltime

First arrivals associated with direct travelpaths show no change in traveltime with depth. The inversion of equation (1) or equation (12) is a straightforward method to obtain the propagation velocity. In strata with thin low-velocity layers, for which critical refraction occurs with a relatively high-velocity layer above and is immediately succeeded by critically refracted arrivals from a high-velocity layer below (Rucker and Ferré 2004), no first-arriving direct waves may exist. For a direct arrival to be present, the layer must have a thickness greater than the sum of the two refraction termination depths. For our dipping layer example, we assume that the velocity of the layer below the dip cannot be obtained from a direct arrival, i.e. it is a thin layer. The velocity then has to be estimated by other means.

The slope method used by Rucker and Ferré (2003) relied on knowledge of the higher velocity in which critical refraction along the interface occurs, i.e.

$$v_2 = \frac{2v_1}{\sqrt{\Delta^2 v_1^2 + 4}}, \quad (14)$$

where Δ is the traveltime slope (dt/dz) and v_1 is obtained from the traveltime profile using equation (1). For our example with soil velocities of 0.1 and 0.05 m/ns, the traveltime profile would exhibit a slope of 34.64 ns/m. For comparison with the dipping layers, slopes of different portions of the traveltime profile in Fig. 3(a, b) were calculated, including the region of cross-dip and critical refraction.

Table 1 shows the results of the computed slopes with two different models of the high-velocity layer. Two important conclusions can be drawn from Table 1. First, the dip angle and offset do not affect the slope of the traveltime profile in the region of critical refraction. The slope of both earth models with dip vary only slightly from the slope of the flat-lying layers. This indicates that, regardless of dip, we can use the slope method to calculate the velocity below the dip accurately. Second, the slope of the cross-dip portion is approximately half the slope in the region of critical refraction. The difference in slope will help in identifying the two travelpaths on a traveltime profile.

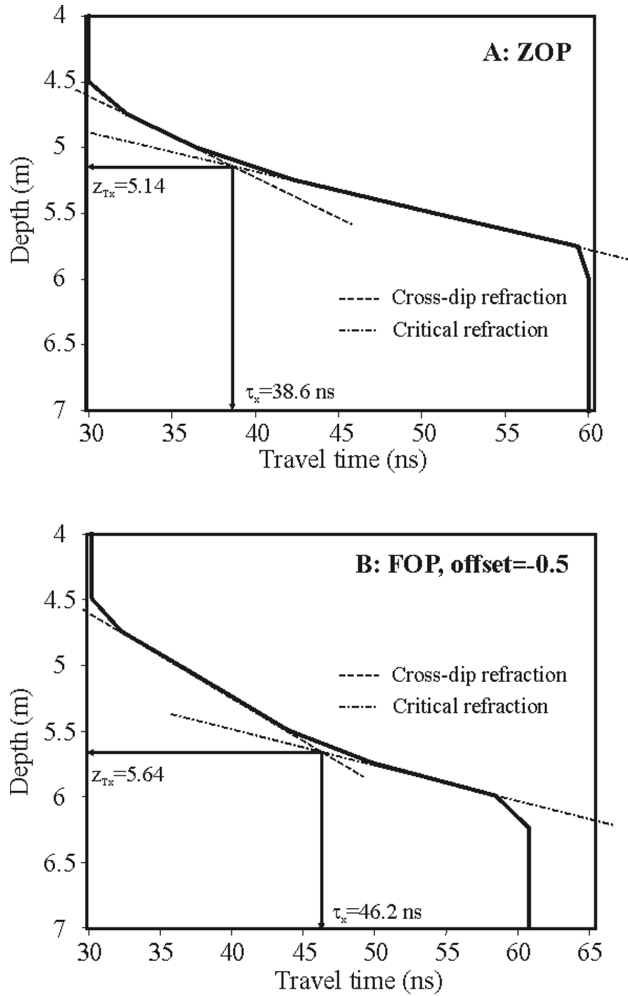


FIGURE 4
Traveltime inversion of a synthetic example to obtain dip angle and dip position. (a) Zero-offset profile with cross-over time. (b) Fixed-offset profile with cross-over time.

To obtain the dip angle and dip position, we consider the traveltime when the receiving antenna is located exactly at the interface and the transmitting antenna is located below the interface. In this configuration, the first-arrival traveltime crosses over from the cross-dip traveltime to the critical refraction traveltime. This cross-over traveltime (τ_x), derived in Appendix B, is given by

$$\tau_x = \frac{z_u v_1 \cos^2(\alpha) - z_u v_2 \sin(\theta_c + \alpha) \cos(\alpha) + v_2 x \cos(\theta_c)}{v_1 v_2 \cos(\theta_c) \cos(\alpha)}. \quad (15)$$

For this case,

$$z_u = -offset, \quad (16)$$

and z_{Tx} is the position of the transmitting antenna when the receiving antenna is located at the interface. Solving for z_{Tx} yields

$$z_{Tx} = z_{dip} - \frac{v_1 v_2 \cos(\theta_c)}{v_1 \cos(\alpha) - v_2 \sin(\theta_c + \alpha)} \tau_x + 2 \quad (17)$$

$$\frac{v_2 x \cos(\theta_c)}{\cos(\alpha)} - v_2 x \sin(\theta_c + \alpha) \tan(\alpha) + v_1 x \sin(\alpha) = \frac{v_1 \cos(\alpha) - v_2 \sin(\theta_c + \alpha)}{v_1 \cos(\alpha) - v_2 \sin(\theta_c + \alpha)}.$$

Equation (17) contains two unknowns: z_{dip} and α . Subtracting equation (17) from itself with different values for *offset*, z_{Tx} and τ_x , and solving for α will yield a good approximation for the dip angle:

$$\alpha \cong \tan^{-1} \left(\frac{\sqrt{v_2^2 \left(v_2^2 - \left(\frac{\Delta z_{Tx}}{\Delta \tau_x} \right)^2 - v_1^2 \right) + \left(\frac{\Delta z_{Tx}}{\Delta \tau_x} \right)^2 v_1^2 - v_2^2}}{v_2 \sqrt{v_2^2 \left(v_2^2 - \left(\frac{\Delta z_{Tx}}{\Delta \tau_x} \right)^2 - v_1^2 \right) + \left(\frac{\Delta z_{Tx}}{\Delta \tau_x} \right)^2 v_1^2} + v_2 \sqrt{v_1^2 - v_2^2}} \right) \quad (18)$$

The value for $\Delta z_{Tx}/\Delta \tau_x$ is obtained directly from the two traveltime profiles. Specifically, the values of z_{Tx} and τ_x can be interpreted by fitting lines to the two traveltime regions of cross-dip and critical refraction. Once the dip angle is computed, the dip position can be obtained readily from equation (17) with information from one profile.

As an example, Fig. 4(a) shows a zero-offset profile with a dip of 10° (identical to Fig. 3a). The traveltimes of the cross-dip and critically refracted regions are identified by straight lines. The point at which the lines intersect demarcates the location of the transmitting antenna when the receiving antenna is at the interface (5.14 m). The cross-over traveltime is 38.6 ns. Figure 4(b) is a fixed-offset profile with an offset of -0.5 m. τ_x is 46.2 ns and z_{Tx} is 5.64 m. The value of $\Delta z_{Tx}/\Delta \tau_x$ is 0.065 m/ns. Using equation (18), the dip angle is approximately 11° , which is very close to the value of 10° used in the forward model. The dip angle, cross-over time, and antenna position from Fig. 4(a) are used in equation (17) to obtain the dip location, z_{dip} , of 4.89 m. The calculated value for z_{dip} is close to the value used in the forward model (4.875 m).

FIELD EXPERIMENT

Borehole ground-penetrating radar, first-arrival travel profiles with zero-offset and a fixed-offset of -0.5 m were collected at a field site in Tucson, Arizona (Fig. 5). The site was located along the bank of the Santa Cruz River, an ephemeral stream that flows from the south to the north through the city. Radar data was collected with a PulseEkko 100 (Sensors and Software, Mississauga, Ontario) borehole radar system with a 100 MHz centre frequency antenna. The traveltime profiles were collected in boreholes C and D which have a separation distance of 2.0 m. The profiles were sampled to 10 m depth with a vertical sampling interval of 0.25 m.

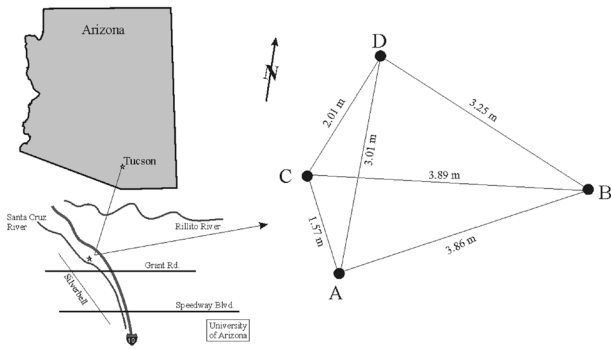


FIGURE 5 Map of experimental site in Tucson, Arizona, showing locations of access tubes for profiling with BGPR.

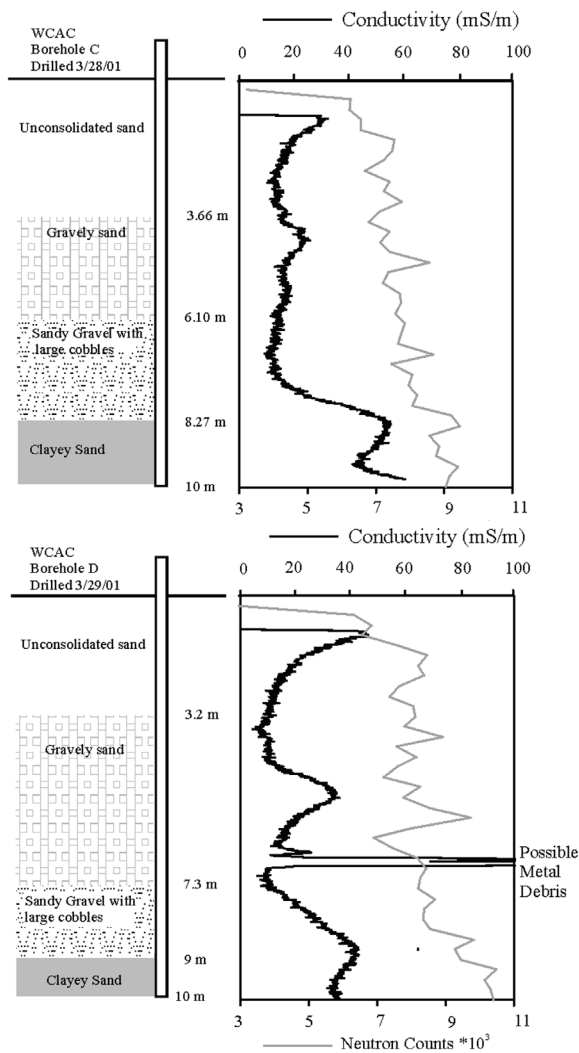


FIGURE 6 Soil type, electrical conductivity [mS/m] log, and neutron count log in boreholes C and D.

A characterization of the sediments from a 20-inch recharge well has been given by Osborne (1969). The well is located approximately 10 m north-east of the present study site, and the completed depth was approximately 45 m. The sediments were characterized using grain-size analysis, and were separated into fines (silt and clay), sand and gravel. For the first 10 m, the section was composed of volcanic samples consisting predominantly of sands and gravels. The fines tended to increase with depth. Caliche cement was also present at around 10 m. Before urbanization and cementation of the riverbank to prevent erosion, the sediments from about 4–10 m were hydraulically connected to the Santa Cruz River (Wilson and de Cook 1968). From approximately 10 m to 25 m, the material was composed of unstained volcanic material and Catalina gneiss with no cementation. The fines continued to increase with depth in this region. From 25 m to 45 m, the older sediments consisted of interbedded deposits of silt, sand and gravel with relatively highly permeable zones in the upper portion. Cementation increased with depth. The water table, at the time of the present study, was located at approximately 35 m.

The BGPR access boreholes were drilled with a 0.2 m (8 inch) bit. The radar access holes were cased with 0.05 m (2 inch) diameter schedule 40 PVC and each was capped at the bottom. The annulus of each borehole was backfilled with well-sorted silica sand which was mixed with cuttings material from the boreholes. The cuttings were sieved with a screen size of 1.25 cm before backfilling. The top 0.45 m was backfilled with a bentonite-sand mixture to help prevent shortcutting of water through the borehole annulus.

For the present study, continuous cores were taken with a split-spoon sampler in all four boreholes (ASTM 1992). The cores were characterized by soil type by inspection. The soil types included clay, sand, gravel and cobbles in any combination. Figure 6 shows the results of soil characterization for boreholes C and D. In general, the top six inches of soil consists of dry, unconsolidated loose sand and silt. The surface material is underlain by a thick (~3.3 m) sandy layer with interspersed lenses of organic material and clay. A black, peat-like organic layer is located approximately 1 m below the surface. The material between 3.3 m and 6.5 m below ground is a gravely sand, and between 6.5 m and 8.5 m, it becomes cobbles, gravel and sand. From about 8.5 m to 12 m, the medium varies from a 1.5-m thick clay lens to rich clayey sand. The remainder of the profile to 15.25 m depth is comprised of fine sand with small amounts of clay.

In addition to the BGPR profiles obtained in boreholes C and D, electromagnetic induction (EMI) and neutron logging were performed. A Model 9512A EMI tool (Century Geophysical Corp., Tulsa, Oklahoma) was used to measure the electrical conductivity. The measurements started at approximately 0.5 m below ground surface and the boreholes were logged at intervals of 0.01 m at a rate of 6 m/min to a depth of 10 m (Fig. 6). The tool can be quite sensitive to possible metallic debris in the annulus, which is seen at about 7 m below ground surface in borehole D.

A neutron probe (Campbell Pacific Nuclear, model 503DR) was used to profile the boreholes to obtain absolute counts of back-scattered thermalized neutrons. The boreholes were logged at intervals of 0.25 m. A 32-second count was performed for each measurement location. Figure 6 shows that, at approximately 8 m, the change in soil type from sandy gravel to clayey sand caused a large change in both the electrical conductivity and the neutron counts. In borehole C, the electrical conductivity increased from about 20 mS/m to 60 mS/m in the interval from 7.75 m to 8.5 m. The neutron count increased from approximately 8500 to 9800 counts in the depth range from 8 m to 8.5 m. The same trend can be seen in borehole D, but the changes in neutron counts and electrical conductivity occur approximately 0.5 m below the depth of change seen in borehole C, indicating that the layer boundary dips. Soil characterization also confirms that a dip may be present at this depth. The clayey sand layer starts at about 8.27 m in borehole C and at 9 m in borehole D. From the soil-core characterization, the dip angle is approximately 20° . From the EMI and neutron log, the dip angle is approximately 14° .

The BGPR first-arrival traveltimes data for the borehole pair CD (Fig. 7) were picked using 'PICKER', which is an automated picking software provided by the manufacturer of the radar system (Sensors and Software, Mississauga, Ontario). Figure 7(a) shows first-arrival traveltimes for both zero-offset and fixed-offset profiles with an offset of -0.5 m for the entire profile to 10 m depth. The sampling interval for Fig. 7(a) is 0.25 m. The profile shows that at around 8.25 m depth, there is an increase in traveltime due to refraction, either cross-dip or critical refraction. The dip is recognized by the two profiles having nearly identical traveltime values. Another possible location for a dipping layer is around 4 m to 5 m, as seen in Fig. 6. Figure 7(b, c) shows an

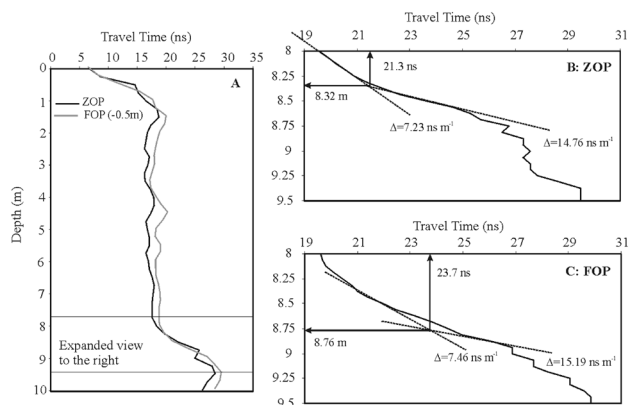


FIGURE 7

First-arrival traveltime profiles in borehole pair CD. (a) zero-offset profile (ZOP) and fixed-offset profile (FOP) traveltimes (-0.5 m offset) for entire profile to 15 m. (b) ZOP traveltime profile from 8 m to 9.5 m showing cross-over time for dip angle and position calculation. (c) FOP traveltime profile from 8 m to 9.5 m showing cross-over time for dip angle and position calculation.

expanded view of the depths from 8 m to 9.5 m, with a sampling interval of 0.0625 ns. From 8 m to 8.75 m, the zero-offset profile (Fig. 7b) shows a traveltime increase that would suggest that a dip exists. The traveltime slope from 8 m to 8.25 m is 7.23 ns/m and the slope from 8.38 m to 8.62 m is 14.76 ns/m . Since the value for the upper slope is approximately half that for the lower slope, these regions represent cross-dip refraction and critical refraction within the profile, respectively. It is assumed that the traveltime at 8 m is from a direct arrival, and the propagation velocity above the dip is 0.102 m/ns using equation (1). The velocity below the dip, using equation (19) and the slope from depths of 8.38 m to 8.62 m is 0.08 m/ns . For the fixed-offset profile (Fig. 7c), the slope from 8.38 m to 8.56 m is 7.46 ns/m and the slope from 8.81 m to 8.94 m is 15.19 ns/m .

To find the cross-over time, τ_x , for each traveltime profile, lines representing the slope were drawn over regions of the traveltime plot that represent cross-dip refraction and critical refraction. The traveltime at which the two lines intersect is τ_x . For Fig. 7(b), the value is 21.3 ns; for Fig. 7(c), the value is 23.7 ns. Using equation (18) and the propagation velocities above and below the dip, we obtain $\Delta z_{\tau_x} / \Delta \tau_x = 0.208 \text{ m/ns}$ and the dip angle, $\alpha = 14^\circ$. Equation (17) was used to determine the dip position, z_{dip} , at 8.4 m. The dip angle is a closer match to the angle predicted from the borehole logs than that from the core characterization. Since the soil samples are not nearly as accurate as borehole logging, it is more likely that the actual dip of the layer is closer to 14° than 20° .

CONCLUSIONS

The forward solution for the first-arrival traveltime from zero-offset and fixed-offset profiling with borehole ground-penetrating radar is presented. The solution assumes that the travelpath of an electromagnetic wave can be analysed using ray tracing. Previous solutions to ray tracing of zero-offset profiling (Rucker and Ferré 2003, 2004) only considered flat-lying layers, where two travelpaths were important for proper interpretation of the velocity structure of the subsurface, i.e. direct and critically refracted travelpaths. For dipping structures, where the antennae are on opposite sides of the interface, a third path is necessary to explain the first-arrival traveltime, i.e. a cross-dip refracted path. The traveltime of this path depends upon the angle of incidence at the interface of the dip.

The inversion of first-arrival traveltimes across a dipping interface to obtain the velocities above and below the dip as well as the dip angle and the dip position is also presented. The solution relies on two traveltime profiles obtained from the zero-offset and fixed-offset profiles. It was shown that dip does not significantly affect the slope in the region of critical refraction, where both antennae lie in the layer of low-propagation velocity. Therefore, the slope method of Rucker and Ferré (2003, 2004) can be used to estimate the velocity below the dip. The dip angle and position are obtained by finding the traveltime when one antenna is located exactly on the down-dip interface.

An example of field-collected first-arrival traveltimes data in alluvial deposits along an ephemeral stream is used to show the accuracy of the inverse solution. The field was characterized beforehand by inspection of continuous cores and through borehole logging with an electromagnetic induction tool and a neutron probe. All three methods showed a dipping clayey sand layer existing approximately 8 m to 8.5 m below ground surface. The dip was estimated to be between 14° and 20° from the horizontal over a separation of 2 m. First-arrival traveltimes from a zero-offset profile and a fixed-offset profile (offset = -0.5 m) were collected with a sampling interval of 0.25 m for the entire profile and 0.0625 m for the section between 7.5 m and 10 m. Both profiles were needed to help delineate the dip in the subsurface. The inversion of the traveltimes data revealed that a dip does exist at approximately 8.4 m at an angle of 14°, which corresponds well with the dip angle estimated from the borehole logging tool. The depth of the dip was found to be located halfway between the depths where electrical conductivity increases in boreholes C and D.

ACKNOWLEDGEMENTS

This material is based on work supported by the National Science Foundation under Grant no. 0097171. Additional support was provided by funds from NASA under contract NASA/JPL 1236728. We are also grateful to James Callegary of the U.S. Geological Survey for providing the electrical conductivity data from the EMI logging.

REFERENCES

- Alumbaugh D.L., Chang P.U., Paprocki L., Brainard J., Glass R.J. and Rautman C.A. 2002. Estimating moisture contents in the vadose zone using cross-borehole ground penetrating radar: A study of accuracy and repeatability. *Water Resources Research* **38**, 1309.
- ASTM 1992. *Test Methods for Penetration Test and Split-Barrel Sampling of Soils*, D 1586 – 84. American Society for Testing and Materials, 100 Barr Harbor Drive, West Conshohocken, PA 19428-2959.
- Cai J. and McMechan G.A. 1995. Ray-based synthesis of bistatic ground-penetrating radar profiles. *Geophysics* **60**, 87–96.
- Chan C.Y. and Knight R. 1999. Determining water content and saturation from dielectric measurements in layered materials. *Water Resources Research* **35**, 85–93.
- Davis J.L. and Annan A.P. 1989. Ground-penetrating radar for high-resolution mapping of soil and rock stratigraphy. *Geophysical Prospecting* **37**, 531–551.
- Davis J.L. and Annan A.P. 2002. Ground penetrating radar to measure soil water content. In: *Methods of Soil Analysis Part 4 - Physical Methods* (eds J.H. Dane and G.C. Topp), pp. 446–463. Soil Science Society of America, Madison, WI.
- Day-Lewis F.D., Harris J.M. and Gorelick S.M. 2002. Time-lapse inversion of crosswell radar. *Geophysics* **67**, 1740–1752.
- Holliger K., Musil M. and Maurer H.R. 2001. Ray-based amplitude tomography for crosshole georadar data: A numerical assessment. *Journal of Applied Geophysics* **47**, 285–298.
- Jackson M. and Tweeton D. 1994. *MIGRATOM—Geophysical tomography using wavefront migration and fuzzy constraints*. U.S. Bureau of Mines Report of Investigations RI 9497.
- Lager D.L. and Lytle R.J. 1977. Determining a subsurface electromagnetic profile from high frequency measurements by applying reconstruction technique algorithms. *Radio Science* **12**, 249–260.
- Nekut A.G. 1994. Electromagnetic ray-tracing tomography. *Geophysics* **59**, 371–377.
- Osborne P.S. 1969. *Analysis of well losses pertaining to artificial recharge*. MSc thesis, University of Arizona, Tucson.
- Redman D., Parkin G. and Annan P. 2000. Borehole GPR measurement of water content during an infiltration experiment. *Proceedings of the 8th International Conference on Ground Penetrating Radar*, SPIE Vol. 4084, pp. 501–505.
- Rucker D.F. and Ferré T.P.A. 2003. Near-surface water content estimation with borehole ground penetrating radar using critically refracted waves. *Vadose Zone Journal* **2**, 252–257.
- Rucker D.F. and Ferré T.P.A. 2004. Correcting water content measurement errors associated with critically refracted first-arrivals on zero offset profiling borehole ground penetrating radar profiles. *Vadose Zone Journal* **3**, 278–287.
- Vasco D.W., Peterson D.E.Jr. and Lee J.H. 1997. Ground-penetrating radar velocity tomography in heterogeneous and anisotropic media. *Geophysics* **62**, 1758–1773.
- Wilson L.G. and de Cook K.J. 1968. Field observations on changes in the subsurface water regime during influent seepage in the Santa Cruz River. *Water Resources Research* **4**, 1219–1234.

APPENDIX A

Forward model of cross-dip first-arrival traveltimes

Using the parameters defined in Fig. 2(a), we wish to find the angle of incidence (θ_1) at the dipping plane from a source located in layer v_2 . The entry of the ray is located at x_u from the updip intersection of the transmitter and the planar interface. The length of the dipping interface is

$$x_u + x_d = \frac{x}{\cos \alpha}. \quad (\text{A1})$$

Using the law of sines, x_d and x_u are defined as

$$x_u = \frac{z_u \sin(\theta_1 + \alpha)}{\cos(\theta_1)}, \quad (\text{A2})$$

$$x_d = \frac{z_d \sin(\theta_2 + \alpha)}{\cos(\theta_2)}, \quad (\text{A3})$$

and

$$\theta_2 = \sin^{-1} \left(\frac{v_1}{v_2} \sin(\theta_1) \right). \quad (\text{A4})$$

Substitution of equations (A2)–(A4) into (A1) yields

$$z_u \frac{\sin(\theta_1 + \alpha)}{\cos(\theta_1)} + z_d \frac{\sin \left(\sin^{-1} \left(\frac{v_1}{v_2} \sin(\theta_1) \right) + \alpha \right)}{\sqrt{1 - \frac{v_1^2}{v_2^2} \sin^2(\theta_1)}} - \frac{x}{\cos \alpha} = 0. \quad (\text{A5})$$

For a dip angle of less than approximately 25°, equation (A5) can be approximated by

$$z_u + \frac{z_d}{\sqrt{1 - \frac{v_1^2}{v_2^2} \sin^2(\theta_1)}} - \frac{x}{\cos \alpha} = 0. \quad (\text{A6})$$

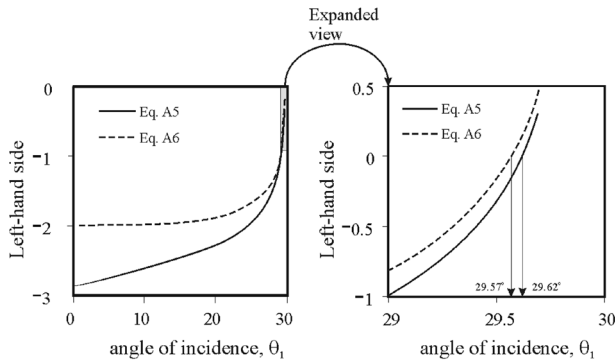


FIGURE 8

Comparison of equations (A5) and (A6) over angles ranging (a) from 0° to the critical angle ($\theta_c=30^\circ$), (b) from 29° to 30° .

Solving for θ_1 yields

$$\theta_1 = \cos^{-1} \left[\left(1 - \frac{v_2^2}{v_1^2} + \frac{v_2^2}{v_1^2} \left(\frac{\cos(\alpha) z_d}{x - z_u \cos(\alpha)} \right)^2 \right)^{1/2} \right]. \quad (\text{A7})$$

Figure 8 shows the graph of the left-hand sides of equations (A5) and (A6) in the vicinity of the solution, from 29° to 29.7° . The difference between the angles calculated from the two solutions is very small, showing that equation (A6) is an acceptable solution.

APPENDIX B

Inversion of traveltimes for dip angle and position

To obtain the two unknown parameters, α and z_{dip} , two traveltimes equations are needed. For simplicity, we use the zero-offset profile traveltimes but two fixed-offset profiles could be used. Additionally, since the slope of the cross-dip traveltimes is significantly different from the slope of the critical refracted traveltimes, a fixed-offset profile with negative offset is used. To calculate the traveltimes when the receiving antenna is located exactly at the interface, the following geometrical conditions are considered:

$$\begin{aligned} \theta_1 &= \theta_c, \\ \theta_2 &= 90^\circ, \end{aligned}$$

$$z_2 = x_d = \frac{x}{\cos(\alpha)} - x_u. \quad (\text{B1})$$

Using equations (2)–(4), the first-arrival traveltimes is

$$\tau_x = \frac{z_u v_1 \cos(\alpha) - z_u v_2 \sin(\theta_c + \alpha) \cos(\alpha) + v_2 x \cos(\theta_c)}{v_1 v_2 \cos(\theta_c) \cos(\alpha)}, \quad (\text{B2})$$

where

$$z_u = z_{\text{Tx}} - z_{\text{dip}} + \frac{x}{2} \tan(\alpha),$$

$$z_{\text{Tx}} = z_{\text{Rx}} - \text{offset} \quad (\text{B3})$$

$$\text{and } z_{\text{Rx}} = z_{\text{dip}} + \frac{x}{2} \tan(\alpha).$$

Substitution of equation (B3) into (B2) and solving for z_{Tx} yields

$$z_{\text{Tx}} = z_{\text{dip}} - \frac{v_1 v_2 \cos(\theta_c)}{v_1 \cos(\alpha) - v_2 \sin(\theta_c + \alpha)} \tau_x \quad (\text{B4})$$

$$+ 2 \frac{\frac{v_2 x \cos(\theta_c)}{\cos(\alpha)} - v_2 x \sin(\theta_c + \alpha) \tan(\alpha) + v_1 x \sin(\alpha)}{v_1 \cos(\alpha) - v_2 \sin(\theta_c + \alpha)}.$$

Subtracting equation (B4) from itself with two pairs of (z_{Tx}, τ_x) yields

$$\frac{\Delta z_{\text{Tx}}}{\Delta \tau_x} = \frac{v_1 v_2 \cos(\theta_c)}{\cos(\alpha) (v_2 \sin(\theta_c + \alpha) - v_1 \cos(\alpha))}. \quad (\text{B5})$$

Expanding equation (B5), where

$$\cos(\theta_c) = \frac{\sqrt{v_1^2 - v_2^2}}{v_1}, \quad \sin(\theta_c) = \frac{v_2}{v_1}, \quad (\text{B6})$$

yields

$$\frac{\Delta z_{\text{Tx}}}{\Delta \tau_x} = \frac{v_1 v_2 \sqrt{v_1^2 - v_2^2}}{\cos(\alpha) \left[(v_1^2 - v_2^2) \cos(\alpha) - v_2 \sqrt{v_1^2 - v_2^2} \sin(\alpha) \right]}. \quad (\text{B7})$$

For small dip angles (less than 20°), the outer cosine of the dip angle in the denominator is approximately 1. With this approximation, the solution for dip angle becomes tractable, i.e.

$$\alpha \cong \tan^{-1} \left(\frac{\sqrt{v_2^2 \left(v_2^2 - \left(\frac{\Delta z_{\text{Tx}}}{\Delta \tau_x} \right)^2 - v_1^2 \right) + \left(\frac{\Delta z_{\text{Tx}}}{\Delta \tau_x} \right)^2 v_1^2 - v_2^2}}{v_2 \sqrt{v_2^2 \left(v_2^2 - \left(\frac{\Delta z_{\text{Tx}}}{\Delta \tau_x} \right)^2 - v_1^2 \right) + \left(\frac{\Delta z_{\text{Tx}}}{\Delta \tau_x} \right)^2 v_1^2} + v_2 \sqrt{v_1^2 - v_2^2}} \right). \quad (\text{B8})$$